

GEOMETRICALLY NONLINEAR ANALYSIS OF PIEZOELECTRIC ACTIVE LAMINATED SHELLS BY MEANS OF ISOGEOMETRIC FE FORMULATION


Predrag Milić¹, Dragan Marinković^{2,3}, Žarko Čojbašić¹

¹University of Niš, Faculty of Mechanical Engineering in Niš, Serbia


²Department of Structural Analysis, TU Berlin, Germany

³Mechanical Science Institute, Vilnius Gediminas Technical University-VILNIUS TECH,
Vilnius, Lithuania

ORCID iDs: Predrag Milić

 <https://orcid.org/0000-0001-7778-6097>

Dragan Marinković

 <https://orcid.org/0000-0002-3583-9434>

Žarko Čojbašić

 <https://orcid.org/0000-0002-4581-1048>

Abstract. *The topic of piezoelectric active thin-walled structures has attracted a great deal of attention over the previous couple of decades. Lightweight structures with piezoelectric material based active elements, sensors and actuators, offer numerous advantages over their passive counterparts. This explains the motivation of authors to dedicate their work to this enticing research field. Accurate and reliable numerical tools for modeling and simulation of this type of structures is still a hot topic in the research community. This paper offers an isogeometric finite element formulation for shell type of structures made of composite laminates including piezoelectric layers characterized by the electro-mechanical coupling. The shell kinematics is based on the Mindlin-Reissner assumptions, thus including the transverse shear effects. A few examples selected from the available literature are considered to demonstrate the applicability of the developed numerical tool and assess its performance.*

Key words: *Isogeometric analysis, Laminated structure, Reissner-Mindlin kinematics, Shell, Piezoelectricity, Geometrically nonlinear analysis*

1. INTRODUCTION

Modern structures are made so as to be fit for their purpose. In order to meet this objective, they are designed to be lightweight. Modern fiber-reinforced composite materials enable design and manufacturing of lightweight structures, while improving the structural performance in different areas – the structures are characterized by high stiffness-to-weight ratio and become less expensive to operate with. Additionally, further improvement

Received: January 05, 2023 / Accepted April 02, 2023

Corresponding author: Predrag Milić

University of Niš, Faculty of Mechanical Engineering in Niš, Aleksandra Medvedeva 14, 18000 Niš, Serbia,

E-mail: predrag.milic@masfak.ni.ac.rs

of structural performance is provided by incorporating active elements made of sophisticated multifunctional materials such as piezoelectric materials [1], shape memory alloys [2], etc. The purpose of adding the active elements is to make the structures adaptive, and such structures are also often popularly referred to as “smart”. In this way, it is aimed at an essential change in their behavior from being only a passive player in the deformational behavior to being an active player that adapts to the current conditions. The structures based on this new paradigm include elements for monitoring structural parameters (sensors), elements that process signals (controllers), and elements that act onto the structure so as to influence their behavior [3]. The application of this type of structures is quite broad, thus covering various fields, including energy harvesting [4], robotics [5], space technologies [6], automotive [7], etc.

A design based on thin walls is the most natural way of producing a lightweight structure, particularly if a structure is made of a fiber-reinforced composite. This approach, on the other hand, may increase lateral flexibility, thus significantly affecting deformational behavior of those structures, especially their dynamic behavior being affected [8]. Hence, the most common objective of adding the active elements is to positively influence the dynamic behavior of these structures with the aim of diminishing their vibrations and thus improve their safety and robustness, reduce noise emission, improve their life span, etc.

The finite element method is currently one of the most advanced methods in the field of structural analysis. In the beginning, the developed elements were aimed at purely mechanical problems. In recent decades, multidisciplinary approaches gained in significance and the developments needed to cover coupled-field problems. The previous two decades have seen numerous developments of robust, accurate and efficient formulations and finite elements for modeling piezoelectric structures characterized by electromechanical coupled field effects [9, 10, 11, 12].

Various 2D theories have been developed and applied to modeling and simulation of thin-walled structures [13]. While the classical laminate theory is appealing due to less nodal degrees of freedom required, the higher order of continuity of the shape functions is the major obstacle in its implementation into the FEM. Despite of that, the issue was addressed in a discretized form by some authors [14]. Most of the authors turned their attention to the first-order shear deformation theory, which is due to both, the better suitability of the theory for laminated structures (prone to the transverse shear effects) and the required C^0 -continuity of the shape functions [15, 16]. Taking an improved accuracy and a more consistent description of the transverse shear effects as the main objectives, some authors based their developments on higher-order shear deformation theories [17, 18]. The numerical effort associated with these theories, which is not far away from the full 3D approach, is the obvious disadvantage. Besides these efforts, the need to cover geometrically nonlinear effects was recognized recently and a number of developments were reported in this direction [19, 20]. Recent papers were dedicated to the co-rotational FE formulation for both passive and active shell structures [21, 22].

Another relatively recent and quite interesting approach is denoted as isogeometric analysis. It is originally proposed by Hughes et al. [23] and aims at seamless integration of the CAD geometry into the FE models. The most distinctive property of this approach is that the actual, i.e. CAD geometry remains unchanged upon the FE discretization. Development of isogeometric FE formulations relying on both the classical laminate theory based on the Kirchhoff-Love kinematics [24, 25], and the first-order shear deformation theory based on the Mindlin-Reissner kinematics [26], were reported. The same is valid for

higher-order theories [27]. Isogeometric FE formulations for composite laminates were also reported [28, 29].

This paper aims at a geometrically nonlinear isogeometric formulation for shell type of structures made of composite laminates with embedded piezoelectric layers that may act both as actuators and sensors. It represents an extension of the recently reported isogeometric development for the same type of structures, but done for linear analysis [30].

2. NURBS GEOMETRY, BASIC FUNCTIONS AND MESH PROPERTIES

CAD description of geometry and, therewith, the isogeometric formulation of finite elements is based on Non-Uniform Rational B-Splines – NURBS. NURBS is a special type of B-spline and, hence, its properties partly depend on the properties of B-spline. To determine the basis functions of the NURBS, it is necessary to define the basis functions of the B-spline first. A clear advantage of NURBS compared to a B-spline resides in its ability of accurate representation of complex geometric shapes.

The basis functions of B-spline of the order zero are determined as:

$$N_{i,0}(\xi) = \begin{cases} 1 & \xi_i \leq \xi < \xi_{i+1} \\ 0 & \text{otherwise} \end{cases} \quad (1)$$

A B-spline of the order p is defined based on the Cox-De Boor's recursive formula. For this purpose, a knot vector $\Xi = [\xi_0, \xi_1, \dots, \xi_{n+p+1}]$ is needed. Higher order basic functions are defined as follows:

$$N_{i,p}(\xi) = \frac{\xi - \xi_i}{\xi_{i+p} - \xi_i} N_{i,p-1}(\xi) + \frac{\xi_{i+p+1} - \xi}{\xi_{i+p+1} - \xi_{i+1}} N_{i+1,p-1}(\xi) \quad (2)$$

A set of parametric coordinates ξ_i given in a non-decreasing order defines the knot vector. The continuity of the basis functions is of great importance and it is defined by the function order, p , and the knot multiplicity, k . A knot multiplicity equals to k implies C^{p-k} continuity. In addition to this, $N_{i,0}(\xi)$ is a stepped function giving non-zero values only in a half-open interval $\xi \in [\xi_i, \xi_{i+1})$. Furthermore, $N_{i,p}(\xi)$ is given by a linear combination of two functions of degree $(p-1)$. A basic function of the order p gives non-zero values only in a half-open interval $\xi \in [\xi_i, \xi_{i+p+1})$ and the sum of all basic functions of the order p at any point ξ is equal to 1. Finally, the basis functions are linearly independent and non-negative.

A NURBS curve of the order p is defined by using the B-spline basis functions and the control polygon points with the corresponding weight coefficients or with control polygon points and their corresponding NURBS basis functions:

$$C(\xi) = \frac{\sum_{i=0}^n N_{i,p}(\xi) w_i P_i}{\sum_{i=0}^n N_{i,p}(\xi) w_i} = \sum_{i=0}^n R_{i,p}(\xi) P_i \quad a \leq \xi \leq b \quad (3)$$

Here, P_i are the control polygon points, w_i the corresponding weights, $\{N_{i,p}(\xi)\}$ the p -order B-spline basic functions defined on the non-uniform knot vector $\Xi = \{a, \dots, a, \xi_{p+1}, \dots,$

$\xi_{m-p-1}, b, \dots, b\}$, while $R_{i,p}$ represent the basic rational functions of the order p that form NURBS.

Typically, the knot vector is normalized. This implies that the first index coordinate of the vector is 0 ($a = 0$), while the last one is 1 ($b = 1$). The number of repetitions of the elements a and b in the knot vector defines the order of spline. Using this parameter, one can realize the discontinuity at the spline ends. Hence, the following equation defines a NURBS surface of the orders p and q in the ξ - and η -directions, respectively:

$$S(\xi, \eta) = \frac{\sum_{i=0}^n \sum_{j=0}^m N_{i,p}(\xi) N_{j,q}(\eta) w_{ij} P_{ij}}{\sum_{k=0}^n \sum_{l=0}^m N_{k,p}(\xi) N_{l,q}(\eta) w_{kl}} = \sum_{i=0}^n \sum_{j=0}^m R_{ij}(\xi, \eta) P_{ij} \quad 0 \leq \xi, \eta \leq 1 \quad (4)$$

where R_{ij} are the rational B-spline basis functions of NURBS surface, i.e. the NURBS basis functions:

$$R_{ij}(\xi, \eta) = \frac{N_{i,p}(\xi) N_{j,q}(\eta) w_{ij}}{\sum_{k=0}^n \sum_{l=0}^m N_{k,p}(\xi) N_{l,q}(\eta) w_{kl}} \quad 0 \leq \xi, \eta \leq 1 \quad (5)$$

Fig. 1 shows an example of a NURBS surface (patch) given by Eq. (4). Points of the control polygon in the physical space, index vectors in the index space and the basic functions order define the shown NURBS surface. The element boundaries are set in the parameter space. The surface belonging to an element is defined on half-open intervals $\xi \in [\xi_i, \xi_{i+1})$ and $\eta \in [\eta_j, \eta_{j+1})$ and they are recognizable after the mapping to the physical space (Fig. 1).

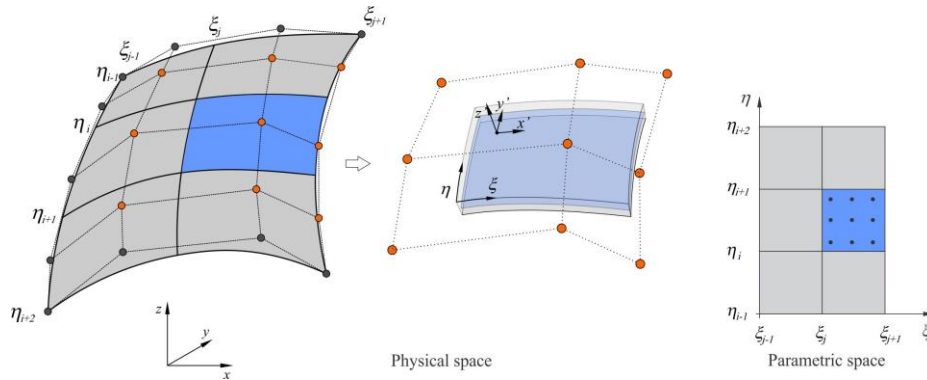


Fig. 1 NURBS surface – mapping between the physical and parametric space

The surface of an element is only a part of the whole patch. It is defined by the necessary mesh parameters, which include control polygon points, weight coefficients and the NURBS basis functions belonging to the half-open intervals $\xi \in [\xi_i, \xi_{i+1})$ and $\eta \in [\eta_j, \eta_{j+1})$. The NURBS basic functions belonging to the points of the patch control polygon outside the observed half-open interval yield a zero value. Consequently, they

have no influence on this part of the geometry. In order to keep track of this fact, all the control points that define the element geometry and their basic functions are numbered from 1 to n_{en} , with $n_{en}=(p+1)(q+1)$.

The initial mesh of finite elements has a total number of finite elements determined by the number of elements in the index vectors and the degrees of the basic functions. It also implies that there is no repetition of elements in the index vectors except at the beginning and the end of the vector:

$$n_e = (n - p)(m - q) \tag{6}$$

Here, m and n are the number of points of the control polygon along the ξ - and η -direction, respectively, while p and q are the basic function degrees in the ξ - and η -directions, respectively. There are several possibilities to change the initial mesh. Knots may be inserted or removed from the knot vectors (h -refinement), the degree of basic functions may be changed (p -refinement) and the degree of basic functions may also be changed followed by insertion of new knots into the knot vectors (k -refinement). The degree of continuity of the basic functions across the elements may be affected by the last mentioned technique.

3. ISOGEOMETRIC SHELL FORMULATION

Four coordinate systems are used in the formulation of the shell isogeometric finite element. Those would be the global Cartesian coordinate system (x, y, z) , the natural coordinate system (r, s, t) with coordinate values $-1 < r, s, t < +1$, the local Cartesian coordinate system (x', y', z') , and the curvilinear coordinate system (ξ, η, ζ) (Fig. 2).

The tangent plane at any point of the surface is given by vectors \vec{V}_{t_1} and \vec{V}_{t_2} determined as derivatives of the position vector r with respect to ξ and η :

$$\begin{aligned} \vec{V}_{t_1} &= \frac{\partial \vec{r}}{\partial \xi} = \sum_{k=1}^{n_m} \frac{\partial R_k(\xi, \eta)}{\partial \xi} P_k \\ \vec{V}_{t_2} &= \frac{\partial \vec{r}}{\partial \eta} = \sum_{k=1}^{n_m} \frac{\partial R_k(\xi, \eta)}{\partial \eta} P_k \end{aligned} \tag{7}$$

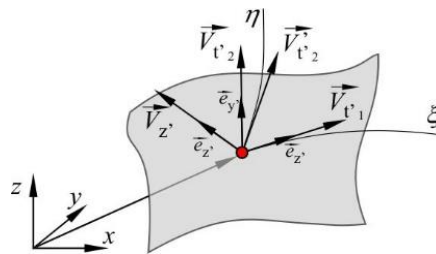


Fig. 2 Coordinate systems used in shell element formulation

Here, $R_k(\xi, \eta)$ are the basic functions and P_k the control polygon points on the element surface. The resulting vectors, \vec{V}_{t_1} and \vec{V}_{t_2} are not perpendicular to each other. In order to

generate an orthogonal coordinate system, the vector product of the obtained two vectors is computed to give a vector normal to the tangent plane.

$$\vec{V}_z' = \vec{V}_{t_1}' \times \vec{V}_{t_2}' \quad (8)$$

The unity vectors of the coordinate system are then easily determined:

$$\vec{V}_{t_2}' = \vec{V}_z' \times \vec{V}_{t_1}' \quad (9)$$

$$\vec{e}_x' = \frac{\vec{V}_{t_1}''}{|\vec{V}_{t_1}''|} = \begin{Bmatrix} l_1'' \\ m_1'' \\ n_1'' \end{Bmatrix}, \vec{e}_y' = \frac{\vec{V}_{t_2}''}{|\vec{V}_{t_2}''|} = \begin{Bmatrix} l_2'' \\ m_2'' \\ n_2'' \end{Bmatrix}, \vec{e}_z' = \frac{\vec{V}_z''}{|\vec{V}_z''|} = \begin{Bmatrix} l_3'' \\ m_3'' \\ n_3'' \end{Bmatrix}, \quad (10)$$

While the definition of the normal to the mid-surface is a trivial task in classical FEM, the isogeometric formulation is somewhat challenging with respect to this aspect. The challenge originates from the fact that the control polygon points are not placed on the actual shell surface and they don't have a unique projection onto the shell surface. The issue has been addressed in the recent work by Milic et al. [30], where several methods from the literature are reported and the approach based on the Greville points [31] is adopted. The same approach is also used in this work.

A point on the structure that is not on the mid-surface is determined by the position vector of its projection onto the mid-surface and with the distance in the direction perpendicular to the mid-surface. The thickness of the shell is determined interpolating the known thicknesses h_k at the polygon control points by means of their corresponding NURBS functions. The position of any point is given as:

$$\begin{Bmatrix} x \\ y \\ z \end{Bmatrix} = \sum_{k=1}^{n_{en}} R_k(\xi, \eta) \left\{ \begin{Bmatrix} x_k \\ y_k \\ z_k \end{Bmatrix} + \frac{h_k}{2} \mathbf{t} \begin{Bmatrix} V_{k3x} \\ V_{k3y} \\ V_{k3z} \end{Bmatrix} \right\} \quad (11)$$

Here, x_k, y_k, z_k represent the control point global coordinates, $V_{k3x}, V_{k3y}, V_{k3z}$ are the components of the vector normal to the mid-surface at control point P_k .

The same shape functions are applied to interpolate the displacement field and define the element geometry. Hence:

$$\begin{Bmatrix} u \\ v \\ w \end{Bmatrix} = \sum_{k=1}^{n_{en}} R_k \left\{ \begin{Bmatrix} u_k \\ v_k \\ w_k \end{Bmatrix} + \begin{Bmatrix} u_k^R \\ v_k^R \\ w_k^R \end{Bmatrix} \right\} \quad (12)$$

Here, u_k, v_k and w_k are the control point displacements in the x -, y - and z directions respectively, while u_k^R, v_k^R and w_k^R denote the relative displacements caused by rotations at the control point k . The latter are to be expressed via the nodal rotations θ_{xk}, θ_{yk} and θ_{zk} , which represent the global rotations.

The Reissner-Mindlin kinematics is applied to determine the relative displacement of any point within the shell with respect to its counterpart on the mid-surface, Those are defined with respect to the local coordinate system at control point k , as follows:

$$\begin{Bmatrix} u_k^R \\ v_k^R \\ w_k^R \end{Bmatrix} = \frac{h_k}{2} t \begin{bmatrix} -\vec{V}_{k2}, \vec{V}_{kl} \end{bmatrix} \begin{bmatrix} \vec{V}_{kl} \\ \vec{V}_{k2} \end{bmatrix} \begin{Bmatrix} \theta_{xk} \\ \theta_{yk} \\ \theta_{zk} \end{Bmatrix} = \frac{h_k}{2} t \begin{bmatrix} -\vec{V}_{k2}, \vec{V}_{kl} \end{bmatrix} \begin{Bmatrix} \theta_{x'k} \\ \theta_{y'k} \end{Bmatrix} \quad (13)$$

Here $\theta_{x'k}$ and $\theta_{y'k}$ are the nodal rotations with respect to the x' - and y' -axis Fig. 4.

Material properties of composite laminates (Fig. 3) are directionally dependent. This fact calls for the definition of the strain field with respect to the local coordinate system. This is commonly done so that a distinction is made between the in-plane components (membrane-flexural strains) and the out-of-plane components (transverse shear), as given below:

$$\{\boldsymbol{\varepsilon}'\} = \begin{Bmatrix} \{\boldsymbol{\varepsilon}'_{mf}\} \\ \{\boldsymbol{\varepsilon}'_s\} \end{Bmatrix} = \begin{Bmatrix} \boldsymbol{\varepsilon}_{x'x'} \\ \boldsymbol{\varepsilon}_{y'y'} \\ \gamma_{x'y'} \\ \gamma_{y'z'} \\ \gamma_{x'z'} \end{Bmatrix} = \begin{Bmatrix} \frac{\partial u'}{\partial x'} \\ \frac{\partial v'}{\partial y'} \\ \frac{\partial u'}{\partial y'} + \frac{\partial v'}{\partial x'} \\ - \\ \frac{\partial v'}{\partial z'} + \frac{\partial w'}{\partial y'} \\ \frac{\partial u'}{\partial z'} + \frac{\partial w'}{\partial x'} \end{Bmatrix} \quad (14)$$

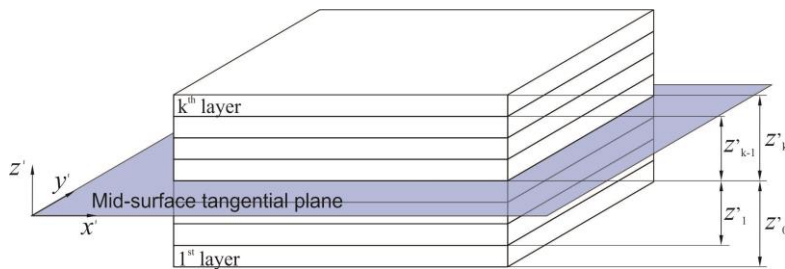


Fig. 3 Laminated structure

The derivatives of the local displacements with respect to the local coordinates are obtained from the derivatives of the global displacements in the global coordinate system by means of the transformation matrix:

$$\begin{bmatrix} u'_{,x'} & v'_{,y'} & w'_{,x'} \\ u'_{,y'} & v'_{,y'} & w'_{,y'} \\ u'_{,z'} & v'_{,z'} & w'_{,z'} \end{bmatrix} = \begin{bmatrix} \vec{V}_{k1} \\ \vec{V}_{k2} \\ \vec{V}_{k3} \end{bmatrix} \begin{bmatrix} u_{,x} & v_{,x} & w_{,x} \\ u_{,y} & v_{,y} & w_{,y} \\ u_{,z} & v_{,z} & w_{,z} \end{bmatrix} \begin{bmatrix} \vec{V}_{k1} & \vec{V}_{k2} & \vec{V}_{k3} \end{bmatrix} \quad (17)$$

where, for instance, $u'_{,x'} = \partial u' / \partial x'$ and $u_{,x} = \partial u / \partial x$.

The derivatives are transformed from the natural to the global coordinate system using the Jacobian inverse matrix:

$$[J] = \begin{bmatrix} x_{,\xi} & y_{,\xi} & z_{,\xi} \\ x_{,\eta} & y_{,\eta} & z_{,\eta} \\ x_{,t} & y_{,t} & z_{,t} \end{bmatrix} = \sum_{k=1}^{n_{en}} \begin{bmatrix} \frac{\partial N_k}{\partial \xi} x_k & \frac{\partial N_k}{\partial \xi} y_k & \frac{\partial N_k}{\partial \xi} z_k \\ \frac{\partial N_k}{\partial \eta} x_k & \frac{\partial N_k}{\partial \eta} y_k & \frac{\partial N_k}{\partial \eta} z_k \\ \frac{h_k}{2} N_k V_{k3x} & \frac{h_k}{2} N_k V_{k3y} & \frac{h_k}{2} N_k V_{k3z} \end{bmatrix} \quad (18)$$

$$\begin{bmatrix} u_{,x} & v_{,x} & w_{,x} \\ u_{,y} & v_{,y} & w_{,y} \\ u_{,z} & v_{,z} & w_{,z} \end{bmatrix} = [J]^{-1} \begin{bmatrix} u_{,\xi} & v_{,\xi} & w_{,\xi} \\ u_{,\eta} & v_{,\eta} & w_{,\eta} \\ u_{,t} & v_{,t} & w_{,t} \end{bmatrix} \quad (19)$$

Upon all the mentioned transformations, the strain field given in Eq. (16) has the following form:

$$\{\varepsilon'\} = [B_u] \{u\} = \begin{bmatrix} [B_{mf}] \\ - \\ [B_s] \end{bmatrix} \{u\} = \begin{bmatrix} [B_{Tm}] & | & t[B_{Rf}] \\ - & + & - \\ [B_{Ts}] & | & [B_{R0s}] + t[B_{R1s}] \end{bmatrix} \left\{ \begin{array}{l} \{u_T\} \\ - \\ \{u_R\} \end{array} \right\} \quad (20)$$

The element strain–displacement matrix, $[B_u]$ consists of the membrane-flexural, $[B_{mf}]$, and transverse shear, $[B_s]$, strain–displacement matrices, which further involve translations and rotations related parts (denoted by T and R in the subscript).

4. CONSTITUTIVE RELATIONS OF PIEZOLAYERS

The form of piezoelectric constitutive equations depends on the choice of independent variables. Within the framework of FEM, the strain and the electric field are the usual choice, thus yielding the matrix form of piezoelectric constitutive equations:

$$\begin{aligned} \{\sigma\} &= [C^E] \{\varepsilon\} - [e]^T \{E\} \\ \{D\} &= [e] \{\varepsilon\} - [d^e] \{E\} \end{aligned} \quad (21)$$

Here $\{\sigma\}$ and $\{\varepsilon\}$ are the mechanical stress and strain in the Voigt notation, respectively, $[C^E]$ is the symmetric material constitutive (Hook's) matrix, $\{D\}$ and $\{E\}$ are the dielectric displacement and the electric field vector, respectively, $[e]$ is the piezoelectric coupling matrix, and $[d^e]$ is the vector of dielectric constants.

For quite thin piezopatches, it has been shown that the electric field may be assumed to be constant over the thickness of the piezolayers [32]. Hence, for the k^{th} piezolayer:

$$E_k = \frac{\Delta\Phi_k}{h_k} \quad (22)$$

where $\Delta\Phi_k$ is the difference of electric potentials between the electrodes of the k^{th} piezolayer and h_k is the thickness of the piezolayer. The resulting electric field – electric potential matrix has a quite simple, diagonal form:

$$B_\phi = \begin{bmatrix} \ddots & & & \\ & \ddots & & \\ & & \frac{1}{h_k} & \\ & & & \ddots \end{bmatrix} \quad (23)$$

5. GEOMETRICALLY NONLINEAR FINITE ELEMENT ANALYSIS

Linear structural analysis resides on the assumption that the displacements are relatively small compared to the dimensions of the modeled structure, while the material behavior is also linear. Also, the boundary conditions must remain unchanged over the course of deformation. On the other hand, geometrically nonlinear analysis takes into account the change in structural configuration during the deformation. Deformation of the structure leads to a change in structural parameters. Considering the fact that the structural deformation progresses continuously, the structural parameters also change are continuously. In each structural configuration, it is necessary to establish the equilibrium between the generalized internal and external forces.

The solution of a nonlinear analysis is sought in a step-by-step approach. If the equilibrium of the system at time t is known, a solution at time $t+\Delta t$ is sought with a suitably chosen time step Δt . Even in a static analysis, a label t is established as an auxiliary variable that indicates the progress of the load level. A set of linearized FE equations for the piezoelectric continuum are given on the element level as follows:

$$\begin{aligned} {}^t[K_{uu}]^t \{\Delta u_e\} + {}^t[K_{u\phi}]^t \{\Delta\bar{\Phi}_e\} &= {}^{t+\Delta t}\{f_{ext_e}\} - {}^t\{f_{int_e}\} \\ {}^t[K_{\phi u}]^t \{\Delta u_e\} + {}^t[K_{\phi\phi}]^t \{\Delta\bar{\Phi}_e\} &= {}^{t+\Delta t}\{q_{ext_e}\} - {}^t\{q_{int_e}\} \end{aligned} \quad (24)$$

Here, $\{f_{ext_e}\}$, $\{f_{int_e}\}$, $\{q_{ext_e}\}$ and $\{q_{int_e}\}$ are the external and internal mechanical and electrical loads, $[K_{uu}]$, $[K_{u\phi}]$ and $[K_{\phi\phi}]$ are the tangential mechanical stiffness, piezoelectric coupling and dielectric stiffness matrices, respectively, while the vectors $\{u_e\}$ and $\{\bar{\Phi}_e\}$ include the mechanical and electrical degrees of freedom of the element, respectively. All the terms are defined for time t , which is denoted by the left superscript, and Δ is used to denote the

increment of the corresponding quantity between two configurations. The external excitations are the applied forces/moments and electrical charges. Their internal counterparts are obtained by integrating the mechanical stresses and dielectric displacements over the current configuration of the structure, respectively:

$${}^t \{f_{int_e}\} = \int_{{}^t V} {}^t [B_L] {}^t \{\sigma\} dV \quad (25)$$

$${}^t \{q_{int_e}\} = \int_{{}^t A} {}^t [B_\phi] {}^t \{D\} dA \quad (26)$$

The integration in Eq. (25) runs over the whole structure, V , while in Eq. (26) only over the surface of the piezopatches, A .

Updated Lagrangian formulation is used in this work and, hence, all the vectors and matrices use the last determined configuration as a reference configuration. The tangential stiffness matrix is computed using the following equation:

$${}^t [K_{int}] = \int_{{}^t V} {}^t [B_u] {}^t [C^E] {}^t [B_u] dV + \int_{{}^t V} {}^t [G] {}^t [\sigma] {}^t [G] dV \quad (27)$$

where ${}^t [G]$ is the matrix of partial derivatives and ${}^t [\sigma]$ is the Cauchy stress tensor:

$$\{g\} = \left\{ \frac{\partial}{\partial x} \quad \frac{\partial}{\partial y} \quad \frac{\partial}{\partial z} \right\}^T \Rightarrow [G] = \begin{bmatrix} \{g\} & \{0\} & \{0\} \\ \{0\} & \{g\} & \{0\} \\ \{0\} & \{0\} & \{g\} \end{bmatrix} \quad (28)$$

$$[\bar{\sigma}] = \begin{bmatrix} \sigma_{xx} & \sigma_{xy} & \sigma_{xz} \\ \sigma_{xy} & \sigma_{yy} & \sigma_{yz} \\ \sigma_{xz} & \sigma_{yz} & \sigma_{zz} \end{bmatrix} \Rightarrow [\sigma] = \begin{bmatrix} [\bar{\sigma}] & [0] & [0] \\ [0] & [\bar{\sigma}] & [0] \\ [0] & [0] & [\bar{\sigma}] \end{bmatrix} \quad (29)$$

The piezoelectric stiffness matrix, $[K_{u\phi}]$, and the dielectric stiffness matrix, $[K_{\phi\phi}]$, are computed in the same manner as in the linear analysis, with the only difference that they are integration over the current volume of the structure:

$${}^t [K_{\phi\phi}] = - \int_{{}^t V} {}^t [B_\phi] {}^t [d^E] {}^t [B_\phi] dV \quad (30)$$

$${}^t [K_{u\phi}] = - \int_{{}^t V} {}^t [B_u] {}^t [e] {}^t [B_\phi] dV = {}^t [K_{\phi u}]^T \quad (31)$$

It should be emphasized that the piezo-electrically induced loads are configuration dependent. They are obtained by multiplying the piezoelectric coupling matrix, Eq. (31), with the electric potential.

The obtained nonlinear problem is resolved by means of the Newton–Raphson iterative procedure [33].

6. NUMERICAL EXAMPLES

In this section, a few selected numerical examples of laminar piezo-electric shells under different load sets are considered. Both the actuator and sensor role of piezoelectric layers are covered.

6.1. Nonlinear analysis of a plate

The in-plane dimension of considered plate are 40×40 mm, while the thickness varies in the considered cases. The structure was discretized using the following finite elements: Shell91 (Ansys), ACSHELL9 [34] and the developed formulation (NURBS). In its initial geometry, the structure is flat, but becomes curved after the first loading step. First, the results of linear and geometrically nonlinear analysis of the plate made of only one piezoelectric ceramic isotropic layer PZT G1195 (properties in Table 1) with different types of finite elements are compared. The structure is exposed to an external force of 24 kN in all considered cases. In the first two cases, the force is distributed over a 40 mm long line (600 kN/m) and in the third case, it is a concentrated force (Fig. 5).

Table 1 Material properties [34]

Material properties	PZT G1195 piezolayer	T300/976 graphite/epoxy
Elastic properties		
Y_{11} (GPa)	63	150
Y_{22} (GPa)	63	9
ν_{12}	0.3	0.3
G_{12} (GPa)	24.2	7.1
Piezoelectric properties		
e_{31} (10^{-5} C/mm ²)	2.286	0
e_{32} (10^{-5} C/mm ²)	2.286	0

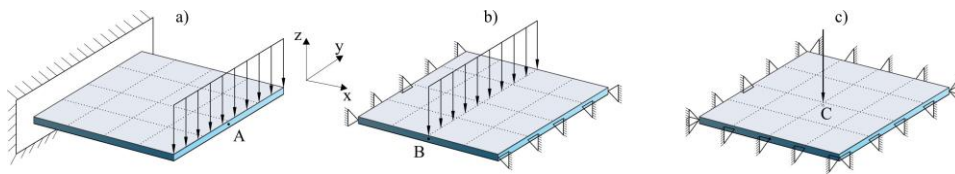


Fig. 5 Initial flat structures, boundary conditions and loads

Figure 5 shows the three models of the considered plate. Due to the kinematic and dynamic boundary conditions, the maximal displacement in the first case would be larger than in the latter two for the same material properties and the thickness. The first model is a clamped plate with a thickness of 5 mm with a load at the free end. The thickness of the plate is chosen so that an obvious non-linear effect occurs. The results of linear and non-linear analysis of this model are given in Fig. 6. Fig. 6a shows the vertical displacement of the free edge mid-point (point A), while Fig. 6b gives its displacement in the x -direction. The latter result is equal to zero in the linear analysis.

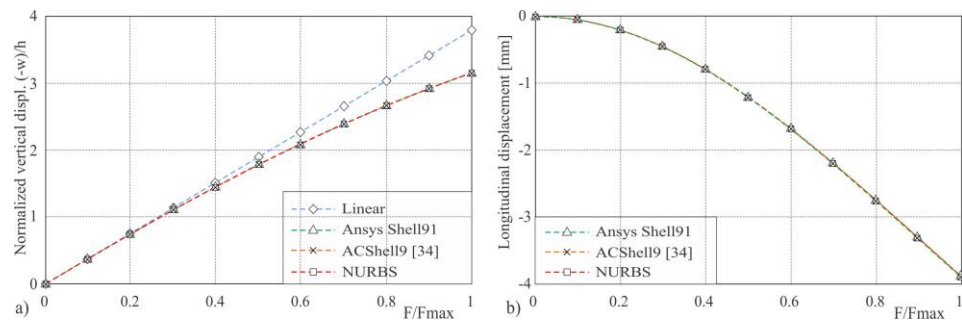


Fig. 6 Clamped structure-displacement of free edge mid-point in: a) vertical direction, and b) in longitudinal (x -)direction

The latter two cases deal with the structure simply supported over the opposite two edges and with the structure simply supported over all four edges. The position of the load was chosen adequately so that, in the first case, it is a line distributed force acting over the middle span width and, in the second case, it is a concentrated force acting at the structure mid-point. Due to the boundary conditions, the structural behavior is significantly stiffer compared to the first case. In order to have geometrically nonlinear effects, a smaller thickness of 3 mm is chosen. In the second example, point B, i.e. the free edge mid-point is chosen as the point with the largest transverse displacement. The maximal transverse displacement of point B in linear and nonlinear analysis is given in Fig. 7a. The linear result for the displacement in x - and y -direction of any point of the plate is zero. However, the nonlinear analysis gives a non-zero displacement in the y -direction, as shown in Fig. 7b.

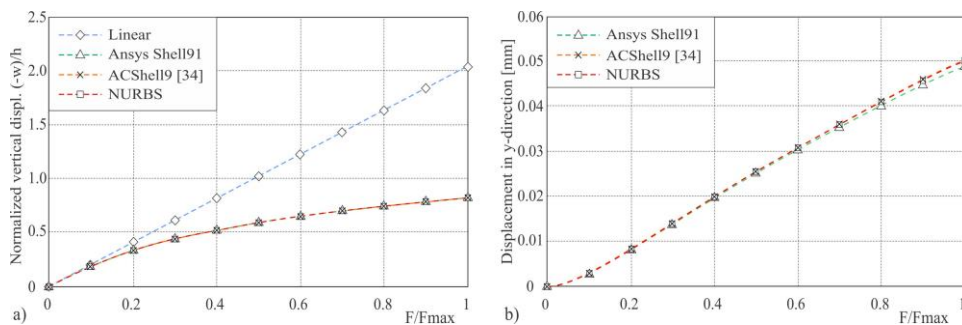


Fig. 7 2-edge-simply supported structure displacement of free edge mid-point in: a) vertical direction and b) in longitudinal (y -)direction

In the case of a structure with four simply supported edges, the mid-point of the plate (point C) was chosen as the reference, Fig. 5c. Due to the susceptibility to shear locking effect of the Ansys Shell91 element, the initial mesh (4×4) was corrected to 20×20 elements to provide accuracy comparable with the ACShell9 and NURBS finite elements, which use a 4×4 mesh. Both, linear and nonlinear prediction yield only the transverse deflection of the observed point Fig 8.

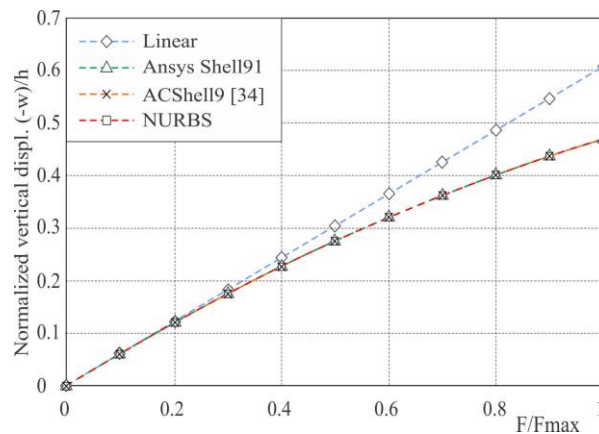


Fig. 8 4-edges-simply supported structure: structure mid-point vertical displacement

In all three considered cases the initial geometry is a plate and the applied loads are such that the linear prediction involves only flexural and shearing strains (no membrane strains). However, with progressing nonlinearity, the membrane strains are also induced as the configuration changes are taken into account. It is obvious and expected that the effect of nonlinearity is the least pronounced in the case of a clamped structure. The model with the NURBS elements in the previously shown examples has a very good agreement with the results obtained with the other considered elements.

The first two plate models are further used to illustrate piezoelectric actuation of the structure in the realm of nonlinear deformations. The observed structures are considered to be made of three layers. The outer layers are made of PZT material (Tab. 1) and the middle layer is made of graphite-epoxy material with a fiber orientation of 90° with respect to the global x -axis. Given that the piezo layer has a relatively small actuation, the aforementioned models should be modified in order to produce a geometrically nonlinear effect. For this reason, a thickness of 0.15 mm is assigned to the piezo layers and the thickness of 0.2 mm to the composite layer. The piezolayers are oppositely polarized, so that their actuation forms a moment equally distributed along the edges of the plate. A voltage of 300V is supplied to both piezolayers. The fiber orientation is chosen so that the structure has a lower bending stiffness about the y -axis than the bending stiffness about the x -axis.

The induced piezo-electric coupling forces are configuration dependent. The new increment of the actuating bending moments is calculated based on the piezo-electric coupling stiffness matrix by performing its integration over the actual structural configuration. The direction and intensity of the induced loads depends on the current configuration (follower forces). The follower nature of the induced forces/moments demands small increments [33] of the electric voltage.

An approximate approach is also used by treating the cases as purely mechanical with the loads that are not of the follower type. To achieve this, a full voltage of 300 V is applied to the initial structure and the bending moments are computed. The calculated moment is then applied in increments. The calculations done with the ACShell9 and NURBS finite element yield small differences (in the order of 10^{-1} %).

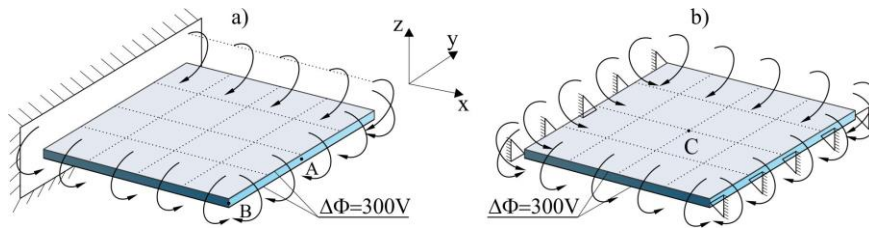


Fig. 9 Initial geometry and boundary conditions

The diagrams in Fig. 10 are obtained by means of the ACShell9 and NURBS diagrams using incremental voltages. The purely mechanical case with the predefined moments is computed using the Shell91 element. Those results are also included in the diagrams. In the clamped structure model (Fig. 9a), two points, A and B, on the structure are chosen to monitor their motion with respect to the gradually increasing excitation. Figs. 10a and 10b depict the transverse deflection and the displacement in the x -direction of the point A. Fig. 11 shows equivalent results to those given in Fig. 10, but for point B of the structure.

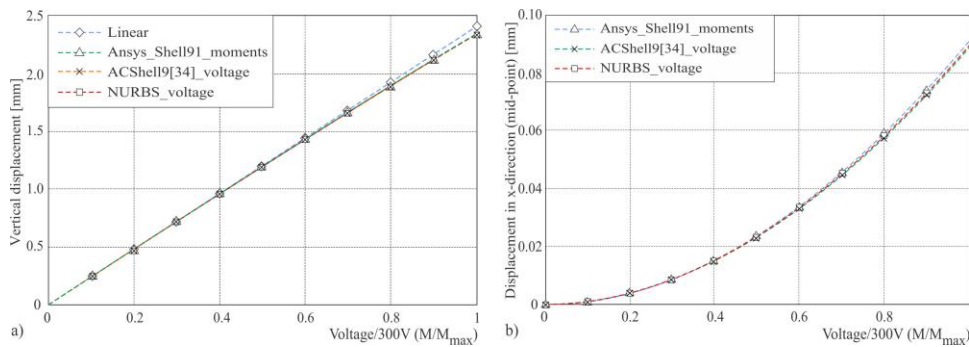


Fig. 10 Clamped piezoelectric plate, point A displacements: a) y -direction; b) x -direction

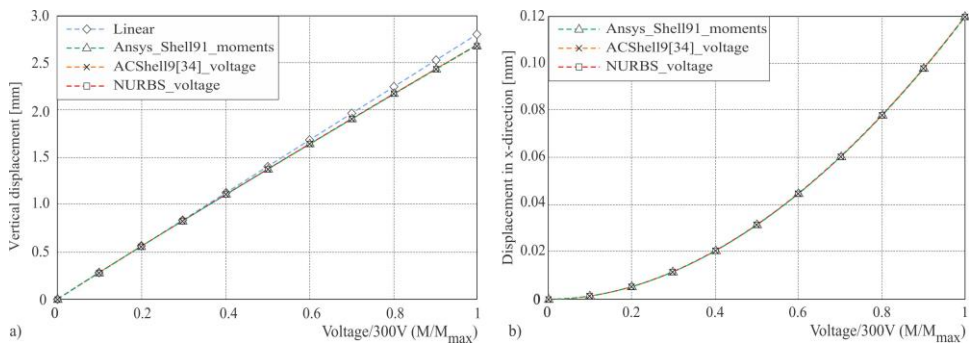


Fig. 11 Clamped piezoelectric plate, point B displacements: a) y -direction; b) x -direction

The previously discussed example reveals a small nonlinear effect on the displacements in the transverse deflection. Fig. 12 gives the results for the transverse deflection in the case

shown in Fig. 9b. Obviously, the difference between the linear and nonlinear results is significantly larger in this case, which is the consequence of more pronounced nonlinear effect through the induced membrane strains and stresses.

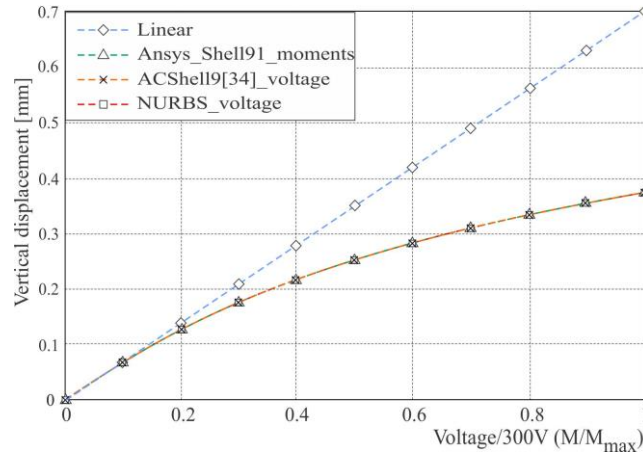


Fig. 12 2-edges-simply supported piezoelectric structure: displacement of point C in the vertical direction

Observing the results of the examples shown, a negligible difference can be observed between the application of elements in which the voltage was applied incrementally (ACShell9, NURBS) and elements, in which the precomputed moment was applied incrementally (Ansys Shell91). This should not lead to a general conclusion in the same direction.

6.2. Nonlinear analysis of piezo-laminated semicircular arch

In the next example, a composite cylinder arc was considered. The structure is formed from three layers. The middle passive layer is made of metal with a thickness of 5.842 mm ($Y=68.95$ GPa, $\nu=0.3$, $\rho=7750$ kg/m³). The outer layers are piezoelectric layers with a thickness of 0.254 mm ($Y=63$ GPa, $\nu=0.3$, $\rho=7600$ kg/m³, $e_{31}=e_{32}=16.11$ C/m², $d_{33}=1.65 \cdot 10^{-8}$ F/m).

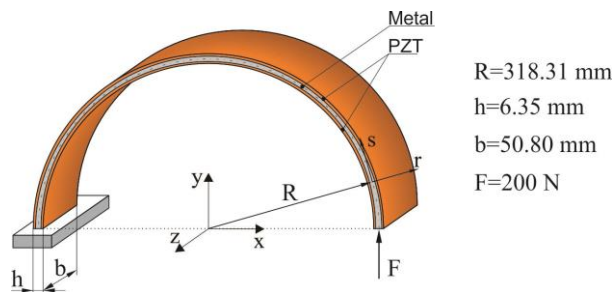


Fig. 13 Piezo-laminated semicircular arch

Only one force F , the magnitude of which is 100 N, acts onto the structure in the middle of the tip of the free edge. The response of the structure in the nonlinear static analysis under the action of the force F was observed through the displacement of the tip of the free edge in the radial direction as well as in the circular direction. The acting force also induces electric voltages in the piezoelectric layers. The voltage of the inner piezoelectric layer is observed for the comparison purposes with the results from the literature. Actually, Tzou and Ye [35] proposed the example originally. It was further modified by Zhang [36], and Marinkovic et al. [22]. Zhang discretized the structure with 10 elements and using one element in the width direction. The model by Marinkovic et al. [22] model uses 160 triangle elements. The NURBS model was formed with quadratic basic functions, with 4 elements in the width direction and 20 elements in the hoop direction. The displacements are shown in Fig. 14 and the induced electric potentials of the inner piezolayer are given in Fig. 15.

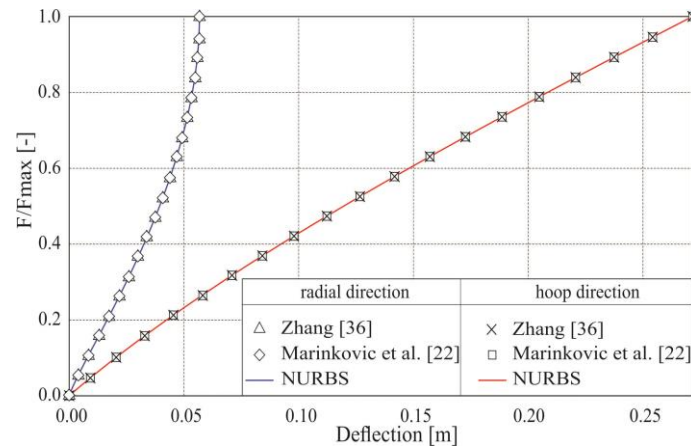


Fig. 14 Displacement of the free arc edge tip in the radial and hoop directions

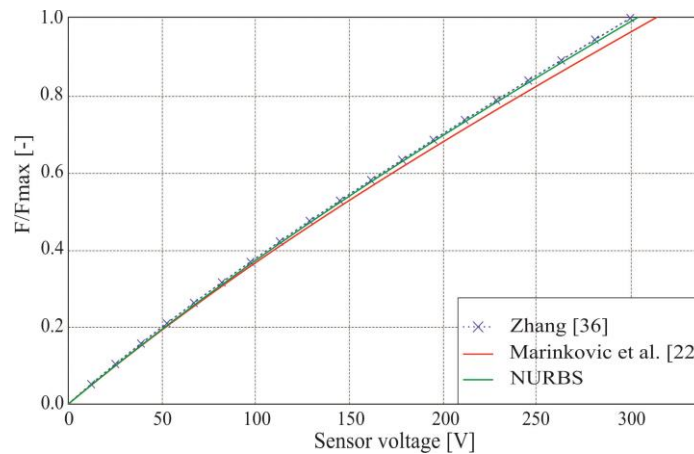


Fig. 15 Sensor voltage of the inner piezolayer

Minor differences between the results for the induced electric potential in the inner piezolayer can be noticed in Fig. 15. This can be attributed to different meshes applied and also the fact that Zhang [36] used the rigorous geometrically nonlinear formulation, while Marinkovic et al. [22] used a co-rotational formulation.

7. CONCLUSIONS

Shell type of structures, i.e. thin-walled structures represent a natural way of achieving lightweight design. In addition to this, novel structural materials, such as fiber-reinforced laminates with high stiffness-to-weight ratio, are used to produce even lighter structures with an option of tailoring material properties by a careful selection of the composite material composition, number and sequence of layers as well as the fiber orientations in the layers. This has been the state-of-the-art in many high performance structures for a few decades. A further improvement comes in the form of adaptive structures – structures provided with active elements, i.e. sensors and actuators, and which can proactively react to different conditions they are exposed to. In the specific case addressed in this paper, the active elements are in the form of thin piezoelectric layers embedded in the laminate structure.

This paper proposed a novel numerical tool for modeling the mentioned type of structures. The finite element method is addressed as the most powerful method in the field of structural analysis. The development is based on a relatively novel isogeometric approach. The main advantage that it offers is a seamless integration of the CAD geometry into the FE model, thus keeping the original, correct geometry of the structure. The proposed formulation covers the mechanical field in the whole structure as well as the electrical field and the piezoelectric coupling in the piezoelectric layers. Thin-walled structures are prone to deformations characterized by large local rotations whereby the strains remain small. For that reason, the developed tool covers both linear and geometrically nonlinear analysis. For the mechanical field, an equivalent single layer approach based on the First-order Shear Deformation Theory is applied.

The considered cases are selected from the available literature in order to have reference solutions. They involve flat and curved structures. But it should be emphasized that although the considered structure is flat in the first set of examples, it is essentially dealt with a shell structure in the geometrically nonlinear analysis as the deformed structure is curved. The computations were done for both purely mechanical and electric excitations. Also, the actuator and sensor function of active layers were covered. It was shown that the proposed formulation successfully covers all the mentioned features and represents a good match for the elements based on the classical FE formulation.

In the future work, the performance of the developed isogeometric formulation with the mesh refinement should be addressed. Also, the formulation should be extended to cover material nonlinearities in the piezoelectric layers that occur at higher voltages.

Acknowledgement: *This research was financially supported by the Ministry of Science, Technological Development and Innovation of the Republic of Serbia (Contract No. 451-03-47/2023-01/ 200109) and by the Science Fund of the Republic of Serbia (Serbian Science and Diaspora Collaboration Program, Grant No. 6497585).*

REFERENCES

1. Wang, K., Alaluf, D., Rodrigues, G., Preumont, A., 2021, *Precision Shape Control of Ultra-thin Shells with Strain Actuators*, Journal of Applied and Computational Mechanics, 7(Special Issue), pp. 1130-1137.
2. Todorov, T., Mitrev, R., Penev, I., 2020, *Force analysis and kinematic optimization of a fluid valve driven by shape memory alloys*, Reports in Mechanical Engineering, 1(1), pp. 61-76.
3. Preumont, A., 2018, *Vibration Control of Active Structures*, Springer Cham, 518 p.
4. Mitrev, R., Todorov, T., Fursov, A., Fomichev, V., Il'in, A., 2021, *A Case Study of Combined Application of Smart Materials in a Thermal Energy Harvester with Vibrating Action*, Journal of Applied and Computational Mechanics, 7(1), pp. 372-381.
5. Nguyen, X., Nguyen, H., 2022, *Investigation of influences of fabrication tolerances on operational characteristics of piezo-actuated stick-slip micro-drives*, Facta Universitatis-Series Mechanical Engineering, 20(1), pp. 109-126.
6. Shao, S., Song, S., Xu, M., Jiang, W., 2018, *Mechanically reconfigurable reflector for future smart space antenna application*, Smart Materials and Structures, 27(9), 095014.
7. Kulkarni, H., Zohaib, K., Khusru, A., Shravan-Aiyappa, K., 2018, *Application of piezoelectric technology in automotive systems*, Materials Today: Proceedings, 5(10, Part 1), pp. 21299-21304.
8. Nestorović, T., Marinković, D., Chandrashekar, G., Marinković, Z., Trajkov, M., 2012, *Implementation of a user defined piezoelectric shell element for analysis of active structures*, Finite Elements in Analysis and Design, 52, pp. 11-22.
9. Rama, G., Marinković, D., Zehn, M., 2018, *Efficient three-node finite shell element for linear and geometrically nonlinear analyses of piezoelectric laminated structures*, Journal of Intelligent Material Systems and Structures, 29(3), pp. 345-357.
10. Carrera, E., Valvano, S., Kulikov, G.M., 2018, *Electro-mechanical analysis of composite and sandwich multilayered structures by shell elements with node-dependent kinematics*, International Journal of Smart and Nano Materials, 9(1), pp. 1-33.
11. Rama, G., Marinkovic, D.Z., Zehn, M.W., 2017, *Linear shell elements for active piezoelectric laminates*, Smart Structures and Systems, 20(6), pp. 729-737.
12. Kulikov, G.M., Plotnikova, S.V., Carrera, E., 2018, *Hybrid-Mixed Solid-Shell Element for Stress Analysis of Laminated Piezoelectric Shells through Higher-Order Theories*, in: Altenbach, H., Carrera, E., Kulikov, G. (Eds), *Analysis and Modelling of Advanced Structures and Smart Systems*, Advanced Structured Materials, vol 81. Springer, Singapore.
13. Reddy, J.N., 2003, *Mechanics of Laminated Composite Plates and Shells: Theory and Analysis*, Second Edition. CRC Press, 858 p.
14. Gabbert, U., Koppe, H., Seeger, F., Berger, H., 2002, *Modelling of smart composite shell structures*, Journal of Theoretical and Applied Mechanics, 3(40), pp. 575-593.
15. Rama, G., Marinkovic, D., Zehn, M., 2018, *A three-node shell element based on the discrete shear gap and assumed natural deviatoric strain approaches*, Journal of the Brazilian Society of Mechanical Sciences and Engineering, 40(7), 356.
16. Petrolo, M., Carrera, E., 2021, *Selection of element-wise shell kinematics using neural networks*, Computers & Structures, 244, 106425.
17. Carrera, E., Zozulya, V.V., 2022, *Carrera unified formulation (CUF) for the micropolar plates and shells. I. Higher order theory*, Mechanics of Advanced Materials and Structures, 29(6), pp. 773-795.
18. Li, G., Carrera, E., Hou, Y., Kulikov, G.M., 2021, *Multi-layered plate finite element models with node-dependent kinematics for smart structures with piezoelectric components*, Chinese Journal of Aeronautics, 34(8), pp. 164-175.
19. Rama, G., Marinkovic, D., 2018, *High performance 3-node shell element for linear and geometrically nonlinear analysis of composite laminates*, Composites Part B: Engineering, 151, pp. 118-126.
20. Katariya, P.V., Hirwani, C.K., Panda, S.K., 2019, *Geometrically nonlinear deflection and stress analysis of skew sandwich shell panel using higher-order theory*, Engineering with Computers, 35, pp. 467-485.
21. Liguori, F.S., Madeo, A., 2021, *A corotational mixed flat shell finite element for the efficient geometrically nonlinear analysis of laminated composite structures*, International Journal for Numerical Methods in Engineering, 122(17), pp. 4575-4608.
22. Marinković, D., Rama, G., Zehn, M., 2019, *Abaqus implementation of a corotational piezoelectric 3-node shell element with drilling degree of freedom*, Facta Universitatis-Series Mechanical Engineering, 17(2), pp. 269- 283.
23. Hughes, T.J.R., Cottrell, J.A., Bazilevs, Y., 2005, *Isogeometric analysis: CAD, finite elements, NURBS, exact geometry and mesh refinement*, Computer Methods in Applied Mechanics and Engineering, 194(39-41), pp. 4135- 4195.

24. Nguyen-Thanh, N., Valizadeh, N., Nguyen, M.N., Nguyen-Xuan, H., Zhuang, X., Areias, P., Zih, G., Bazilevs, Y., De Lorenzis, L., Rabczuk, T., 2015, *An extended isogeometric thin shell analysis based on Kirchhoff-Love theory*, Computer Methods in Applied Mechanics and Engineering, 284, pp. 265-291.
25. Milić, P., Marinković, D., 2015, *Isogeometric FE analysis of complex thin-walled structures*, Transactions of FAMENA, 39(1), pp. 15-26.
26. Benson, D.J., Bazilevs, Y., Hsu, M.C., Hughes, T.J.R., 2010, *Isogeometric shell analysis: The Reissner-Mindlin shell*, Computer Methods in Applied Mechanics and Engineering, 199(5-8), pp. 276-289.
27. Echter, R., Oesterle, B., Bischoff, M., 2013, *A hierarchic family of isogeometric shell finite elements*, Computer Methods in Applied Mechanics and Engineering, 254, pp. 170-180.
28. Yujie, G., Martin, R., 2015, *A layerwise isogeometric approach for NURBS-derived laminate composite shells*, Composite Structures, 124, pp. 300-309.
29. Hosseini, S., Remmers, J.J., Verhoosel, C.V., de Borst, R., 2015, *Propagation of delamination in composite materials with isogeometric continuum shell elements*, Int. J. Numer. Methods Eng., 102(3), pp. 159-179.
30. Milić, P., Marinković, D., Klinge, S., Čojbašić, Ž., 2023, *Reissner-Mindlin based isogeometric finite element formulation for piezoelectric active laminated shells*, Tehnički Vjesnik, 30(2), pp. 416-425.
31. Adam, C., Bouabdallah, S., Zarroug, M., Maitoum, H., 2015, *Improved numerical integration for locking treatment in isogeometric structural elements, Part II: Plates and shells*, Computer Methods in Applied Mechanics and Engineering, 284, pp. 106-137.
32. Marinković, D., Köppe, H., Gabbert, U., 2007, *Accurate modeling of the electric field within piezoelectric layers for active composite structures*. Journal of Intelligent Material Systems and Structures, 18(5), pp. 503-513.
33. Bathe, K.J., 1996, *Finite Element Procedures*, Prentice Hall, New York.
34. Marinković, D., Köppe, H., Gabbert, U., 2008, *Degenerated shell element for geometrically nonlinear analysis of thin-walled piezoelectric active structures*, Smart materials and structures, 17(1), 015030.
35. Tzou, H.S., Ye, R., 1996, *Analysis of piezoelectric structures with laminated piezoelectric triangle shell elements*, AIAA J, 34(1), pp. 110-115.
36. Zhang, S., 2014, *Nonlinear FE Simulation and Active Vibration Control of Piezoelectric Laminated Thin-Walled Smart Structures*, PhD Thesis, Fakultät für Maschinenwesen der Rheinisch-Westfälischen Technischen Hochschule Aachen, Germany, 210 p.